Research Square

Preprints are preliminary reports that have not undergone peer review.
They should not be considered conclusive, used to inform clinical practice,
or referenced by the media as validated information.

Pulmonary Histopathological Findings Following Recurrent Laryngeal Nerve Injury and Reconstruction in Rats: An Experimental Study

Naile Kökbudak

naileyaldiz@hotmail.com

Necmettin Erbakan University

Alper Varman

Necmettin Erbakan University

Ömer Kişi

Necmettin Erbakan University

Zeliha Çelik

Necmettin Erbakan University

Article

Keywords: Recurrent laryngeal nerve, Nerve reconstruction, Fibrin matrix, Lung histopathology, Parenchymal injury

Posted Date: November 2nd, 2026

DOI: https://doi.org/10.21203/rs.3.rs-11232886/v1

License: This work is licensed under a Creative Commons Attribution 4.0 International License.
Read Full License

Additional Declarations: No competing interests reported.

Abstract

Recurrent laryngeal nerve (RLN) injury causes vocal fold paralysis and increases aspiration risk, but the downstream pulmonary histopathological consequences of different repair strategies remain unexplored. In this secondary analysis of tissue from a parent experiment, we compared lung changes after experimental RLN transection among three groups of rats (n = 9/group): unrepaired control, primary end-to-end neurorrhaphy, and neurorrhaphy augmented with donor-derived fibrin matrix. Lungs were harvested at approximately 3 months and nine semi-quantitative parameters were combined into total, parenchymal, and inflammatory injury scores. The total lung injury score differed among groups (P = .003): it was higher after primary repair (median 11.0) than after no repair (8.0; P = .004) or fibrin-augmented repair (8.0; P = .023). Parenchymal injury was higher after primary repair than after no repair, and inflammatory injury was higher after primary repair than after fibrin-augmented repair; pulmonary edema and parenchymal inflammation were the only individual parameters that differed, and bronchial diameter did not. Vocal fold muscle atrophy correlated with the inflammatory score (rho = 0.401, P = .038; exploratory). These findings are hypothesis-generating: the study was not powered for pulmonary outcomes, and whether fibrin-matrix augmentation limits distant pulmonary sequelae requires confirmation in adequately powered studies.

Introduction

Due to its complex and variable anatomical course, the recurrent laryngeal nerve (RLN) remains exceptionally vulnerable to iatrogenic trauma during thyroid and parathyroid surgeries, constituting a frequent subject of surgical malpractice litigation [1,2]. Transection or traction injury of the RLN results in vocal fold paralysis, presenting clinically with hoarseness, dysphonia, dysphagia, and acute or chronic respiratory distress depending on the underlying mechanism, unilateral or bilateral involvement, and anatomical variation [1].

Achieving functional restitution following RLN transection remains among the most formidable challenges in peripheral and cranial nerve reconstruction. In a canine model comparing conventional direct neurorrhaphy, nerve autografts, and bioengineered conduit scaffolds (polyglycolic acid [PGA], acellular matrices), no intervention restored native laryngeal adductor pressure, and bioengineered conduits failed to produce meaningful functional gains [3]. Standardizing functional adductor recovery in animal models remains an ongoing methodological challenge [4]. Although asymmetric porous conduits and microvascular graft transfers have been developed to enhance motor nerve regeneration, their translational applicability remains constrained [5,6].

Consequently, augmenting microsurgical nerve repair with biological matrices or growth factors has garnered substantial interest. In experimental RLN transection models, synthetic PGA conduits elevated distal axonal counts relative to primary suture; however, they concurrently incited pronounced foreign-body reactions, local chronic inflammation, and fascicular disorganization [7]. Reviews of peripheral nerve

scaffolds similarly note that synthetic materials designed to expedite axonal bridging can impose a substantial local inflammatory burden that may compromise functional outcomes [8].

Blood-derived biological products rich in endogenous growth factors, such as platelet-rich plasma, platelet-rich fibrin, and fibrin matrix, offer an appealing alternative. Such products have been reported to accelerate soft-tissue and bony healing in maxillofacial reconstructions [9], and fibrin-based supports have been proposed to facilitate peripheral nerve regeneration [10]. A recent experimental study investigated the effect of platelet-rich plasma injection following RLN injury in rats, reflecting ongoing interest in autologous blood-derived therapies in this setting [11].

At the systemic level, unilateral vocal fold paralysis impairs laryngeal competence and glottic closure, predisposing individuals to tracheobronchial microaspiration; large population-based cohort studies have identified unilateral vocal fold paralysis as an independent risk factor for clinical pneumonia [12,13]. Nevertheless, the downstream pulmonary histopathological changes that occur in lung parenchyma following RLN transection and reconstructive interventions have not been systematically investigated.

The present study evaluated and compared the pulmonary histopathological consequences of three post-transection RLN management strategies in a rat model: unrepaired denervation (control), direct primary neurorrhaphy, and donor-derived fibrin matrix-augmented primary neurorrhaphy. Our primary focus is a morphological, blinded, semi-quantitative histopathological comparison of lung parenchymal and inflammatory architecture across these surgical repair conditions. To our knowledge, this is among the first investigations to systematically evaluate distant target-organ (pulmonary) histopathology within an experimental RLN reconstruction framework.

Results

All 27 rats completed the approximately 3-month postoperative follow-up without premature morbidity or mortality; lung, nerve, and vocal fold specimens from all 27 animals (n = 9 per group) were fully assessable.

Individual Pulmonary Histopathological Parameters

Among the individual histopathological features, pulmonary edema (P = .003) and parenchymal inflammation (P = .004) demonstrated statistically significant differences across groups. Emphysematous changes, atelectasis, peribronchial inflammation, muscular hypertrophy, eosinophil infiltration, and vascular congestion did not show statistically significant intergroup differences (Table 1). Airway obstruction was absent in all animals.

Table 1
Distribution and intergroup comparisons of individual pulmonary histopathological parameters.

Parameter	Group 1 (Control) n (0/1/2); Median [IQR]	Group 2 (Primary Repair) n (0/1/2); Median [IQR]	Group 3 (Fibrin Matrix) n (0/1/2); Median [IQR]	H	p
Emphysematous changes	0/3/6; 2.0 [1.0–2.0]	0/1/8; 2.0 [2.0–2.0]	0/2/7; 2.0 [2.0–2.0]	1.24	0.538
Atelectatic changes	1/5/3; 1.0 [1.0–2.0]	0/3/6; 2.0 [1.0–2.0]	0/5/4; 1.0 [1.0–2.0]	2.41	0.299
Peribronchial inflammation	0/4/5; 2.0 [1.0–2.0]	0/3/6; 2.0 [1.0–2.0]	1/5/3; 1.0 [1.0–2.0]	2.50	0.286
Airway obstruction	9/0/0; 0.0 [0.0–0.0]	9/0/0; 0.0 [0.0–0.0]	9/0/0; 0.0 [0.0–0.0]	-	-
Muscular hypertrophy	6/1/2; 0.0 [0.0–1.0]	5/3/1; 0.0 [0.0–1.0]	4/3/2; 1.0 [0.0–1.0]	0.58	0.747
Pulmonary edema	9/0/0; 0.0 [0.0–0.0]	2/1/6; 2.0 [1.0–2.0]	3/3/3; 1.0 [0.0–2.0]	11.89	0.003
Parenchymal inflammation	6/3/0; 0.0 [0.0–1.0]	2/2/5; 2.0 [1.0–2.0]	8/1/0; 0.0 [0.0–0.0]	10.87	0.004
Eosinophil infiltration	7/2/0; 0.0 [0.0–0.0]	7/2/0; 0.0 [0.0–0.0]	9/0/0; 0.0 [0.0–0.0]	2.26	0.323
Vascular congestion	0/3/6; 2.0 [1.0–2.0]	0/1/8; 2.0 [2.0–2.0]	0/4/5; 2.0 [1.0–2.0]	2.39	0.302

Scores: 0 = absent, 1 = mild, 2 = marked. Animal-based evaluation reflects the worst-affected lung side. Ordinal parameters were compared via the Kruskal-Wallis test (H). Airway obstruction showed no variance and was omitted.

Composite Pulmonary Injury Scores

Analysis of composite scores revealed marked intergroup differences (Table 2). The total lung injury score was significantly elevated in Group 2 (median 11.0, IQR 9.0–12.0) compared with Group 1 (8.0, IQR 7.0–8.0) and Group 3 (8.0, IQR 7.0–9.0; Kruskal-Wallis $P = .003$, $\varepsilon^2 = 0.393$). In pairwise Dunn-Holm comparisons, Group 2 showed significantly greater total injury than Group 1 ($P = .004$) and Group 3 ($P = .023$).

Parenchymal injury scores showed the same trend ($P = .005$), with Group 2 significantly higher than Group 1 ($P = .003$). The inflammatory injury score also differed significantly across groups ($P = .007$), driven by the difference between Group 2 and Group 3 ($P = .005$). Pairwise differences were therefore not uniform across scores: parenchymal injury did not differ significantly between Group 2 and Group 3,

inflammatory injury did not differ significantly between Group 2 and Group 1, and Group 3 showed intermediate parenchymal values (Table 2). Bronchial luminal diameter did not differ significantly (P = .379), indicating that the observed tissue changes occurred independently of macroscopic airway caliber.

Table 2
Composite lung injury scores, lesion burden, and bronchial luminal dimensions.

Outcome	Group 1 (Control) Median [IQR] (Mean ± SD)	Group 2 (Primary Repair) Median [IQR] (Mean ± SD)	Group 3 (Fibrin Matrix) Median [IQR] (Mean ± SD)	H	p	ε²	Significant pairwise comparisons (Holm-adjusted p)
Total lung injury score	8.0 [7.0–8.0] (7.22 ± 1.72)	11.0 [9.0–12.0] (10.67 ± 1.80)	8.0 [7.0–9.0] (7.89 ± 2.03)	11.43	0.003	0.393	G2 > G1, P = .004; G2 > G3, P = .023
Parenchymal injury score	4.0 [4.0–5.0] (4.56 ± 1.01)	7.0 [6.0–8.0] (6.89 ± 1.17)	6.0 [5.0–7.0] (5.78 ± 1.39)	10.74	0.005	0.364	G2 > G1, P = .003
Inflammatory injury score	2.0 [1.0–3.0] (2.11 ± 1.05)	3.0 [3.0–4.0] (3.22 ± 1.20)	1.0 [1.0–2.0] (1.33 ± 0.71)	9.92	0.007	0.330	G2 > G3, P = .005
Marked lesion count	3.0 [1.0–4.0] (2.44 ± 1.51)	4.0 [3.0–6.0] (4.44 ± 1.33)	3.0 [2.0–4.0] (2.67 ± 1.22)	7.26	0.026	0.219	G2 > G1, P = .047
Bilateral marked lesions	1.0 [0.0–2.0] (1.22 ± 1.20)	3.0 [2.0–3.0] (2.67 ± 1.00)	2.0 [1.0–2.0] (1.44 ± 1.01)	6.99	0.030	0.208	G2 > G1, P = .042
Bronchial diameter (mm)	1.70 [1.50–1.75] (1.62 ± 0.33)	1.75 [1.70–2.10] (1.98 ± 0.54)	1.55 [1.45–2.25] (1.77 ± 0.71)	1.94	0.379	0.000	None

ε²: epsilon-squared effect size. Composite scores derived from worst-side evaluations. Pairwise comparisons used Holm-adjusted Dunn tests.

Sensitivity and Bilaterality Analyses

Sensitivity analyses showed that the main finding (higher total lung injury score after primary repair) remained robust across most analytical models (Table 3). Total lung injury scores maintained statistical significance when evaluated using bilateral mean values (P = .003) and isolated left-lung values (P = .002). In the isolated right-lung model, intergroup divergence showed a borderline trend (P = .090), indicating that the overall damage burden was shaped primarily by left-sided and cumulative bilateral injury.

Table 3
Sensitivity analyses for composite pulmonary injury scores across analytical models.

Analytical model	Outcome	Group 1	Group 2	Group 3	H	p	ε^2
Worst-side total score (primary)	Total score	8.0 [7.0–8.0]	11.0 [9.0–12.0]	8.0 [7.0–9.0]	11.43	0.003	0.393
Bilateral average total score	Total score	6.0 [5.5–7.0]	8.5 [8.0–10.0]	7.5 [6.0–7.5]	11.64	0.003	0.402
Isolated right lung total score	Total score	6.0 [4.0–8.0]	9.0 [7.0–10.0]	7.0 [7.0–8.0]	4.81	0.090	0.117
Isolated left lung total score	Total score	6.0 [5.0–7.0]	10.0 [8.0–10.0]	7.0 [5.0–7.0]	12.24	0.002	0.427
Bilateral average parenchymal score	Parenchymal score	3.5 [3.0–4.5]	6.0 [5.0–7.0]	5.5 [4.0–5.5]	9.41	0.009	0.309
Bilateral average inflammatory score	Inflammatory score	2.0 [1.0–2.5]	2.5 [2.0–3.0]	1.0 [1.0–2.0]	8.05	0.018	0.252

Within-animal assessments revealed no significant right-versus-left asymmetry within any group (Wilcoxon signed-rank test P > .05 for all three groups; Table 4). However, Group 2 rats displayed a higher frequency of bilateral marked parameters (median 3.0, IQR 2.0–3.0) and a higher proportion of high bilateral damage (55.6%, n = 5/9) compared with Group 1 (22.2%) and Group 3 (11.1%), indicating a diffuse bilateral pulmonary response in the primary-repair cohort.

Table 4
Intra-animal lung symmetry and bilaterality burden.

Group	Right total score	Left total score	Left-minus-right	Wilcoxon p	Bilateral marked lesions	Bilateral high damage, n (%)
Group 1 (Control)	6.0 [4.0–8.0]	6.0 [5.0–7.0]	1.0 [-1.0–1.0]	0.957	1.0 [0.0–2.0]	2/9 (22.2%)
Group 2 (Primary Repair)	9.0 [7.0–10.0]	10.0 [8.0–10.0]	0.0 [0.0–2.0]	0.313	3.0 [2.0–3.0]	5/9 (55.6%)
Group 3 (Fibrin Matrix)	7.0 [7.0–8.0]	7.0 [5.0–7.0]	-1.0 [-2.0–0.0]	0.188	2.0 [1.0–2.0]	1/9 (11.1%)
Intergroup p	0.090	0.002	0.249	-	0.030	-

Exploratory Correlation Analyses

In exploratory bivariate correlation models, left RLN axonal density showed no significant correlation with total lung injury scores (rho = -0.122, *P* = .545). Similarly, intrinsic vocal fold muscle atrophy (rho = 0.319, *P* = .104) and vocal fold movement (rho = -0.286, *P* = .148) were not significantly correlated with total lung injury scores.

Conversely, a statistically significant, weak-to-moderate positive correlation was observed between intrinsic vocal fold muscle atrophy and the inflammatory lung injury score (rho = 0.401, *P* = .038) (Table 5). While exploratory and not indicative of causality, this finding suggests a possible association between laryngeal muscle denervation-related change and downstream pulmonary inflammatory burden.

Table 5
Exploratory bivariate correlations between neuro-laryngeal parameters and pulmonary injury scores.

Independent variable	Dependent variable	n	Spearman rho	p	Interpretation
Left axonal count	Total lung injury score	27	-0.122	0.545	No significant correlation
Vocal fold muscle atrophy	Total lung injury score	27	0.319	0.104	No significant correlation
Vocal fold mobility	Total lung injury score	27	-0.286	0.148	No significant correlation
Vocal fold muscle atrophy	Inflammatory lung injury score	27	0.401	0.038	Exploratory positive correlation
Vocal fold mobility	Inflammatory lung injury score	27	-0.235	0.238	No significant correlation

Correlation analyses are exploratory and hypothesis-generating and should not be interpreted as evidence of causality.

Discussion

In this experimental study, we evaluated the downstream pulmonary histopathological alterations resulting from three post-transection RLN management strategies in a rat model. The principal finding is that animals undergoing isolated primary neurorrhaphy had a significantly higher total lung injury score than both unrepaired-denervation controls and animals receiving donor-derived fibrin matrix augmentation. The difference was clearest for the total lung injury score and remained robust across most sensitivity models; the component scores were less uniform, with parenchymal injury differing significantly only between primary repair and no repair, and inflammatory injury only between primary repair and fibrin-augmented repair.

Unilateral vocal fold paralysis following RLN injury compromises glottic competence, impairs swallowing coordination, and increases the risk of tracheobronchial aspiration; large clinical cohort studies have identified unilateral vocal fold paralysis as an independent predictor of pneumonia [12,13]. In our series, left vocal fold immobility was endoscopically confirmed in all animals immediately after transection, suggesting that all three groups had a comparable acute-phase aspiration risk, although aspiration itself was not measured. The observation that pulmonary tissue injury differed at approximately 3 months, with higher injury scores in the primary-neurorrhaphy cohort, cannot be explained solely by initial denervation.

One possible explanation involves the neurobiology of nerve regeneration after mechanical coaptation without biological support. It has been proposed that, when a mixed motor nerve such as the RLN is repaired by direct end-to-end suture alone, regenerating axons may be misdirected into antagonistic abductor (posterior cricoarytenoid) and adductor (thyroarytenoid, lateral cricoarytenoid) muscle compartments, a phenomenon discussed in experimental models of laryngeal reinnervation [4]. Such non-selective reinnervation could, in principle, yield less coordinated laryngeal function than complete, static paralysis, in which the immobile vocal fold may be partly compensated for by contralateral mechanisms over time; this remains a proposed mechanism rather than one directly demonstrated in the present study. This interpretation is broadly consistent with our finding of a significant positive correlation between vocal fold muscle atrophy and the inflammatory lung injury score (rho = 0.401, P = .038), which suggests some relationship between laryngeal structural change and downstream pulmonary inflammatory burden; however, our study did not include direct functional or aspiration testing, and this mechanistic interpretation therefore remains speculative and requires dedicated confirmation.

A second, non-mutually-exclusive explanation concerns the local immunomodulatory properties of the fibrin matrix. Blood-derived, growth-factor-rich biological concentrates have been reported to support soft-tissue repair and to modulate local inflammation in other surgical contexts [9,10], and platelet-rich derivatives continue to be investigated for their potential to support neural regeneration after RLN injury

[11]. By providing a biocompatible, blood-derived microenvironment around the microsurgical coaptation, fibrin matrix may reduce foreign-body-type tissue reactivity at the repair site compared with an unsupported suture line, and this local effect could plausibly extend, at least in part, to the lower pulmonary inflammatory scores observed in Group 3 than in Group 2; this proposed mechanism was not directly tested in the present study and should be interpreted with appropriate caution.

These observations are consistent with prior evidence that synthetic or unguided nerve repair materials can provoke substantial local inflammation. In a comparative rat RLN study, PGA-coated conduits achieved higher axonal counts than primary suture alone but also produced marked local inflammation, foreign body reaction, and fascicular disorganization [7]. Such findings indicate that the nature of the regenerative scaffold - whether synthetic or biological - can meaningfully influence tissue remodeling and inflammatory homeostasis, a point also emphasized in reviews of conduit-based nerve repair [8]. The use of a donor-derived fibrin matrix in Group 3 may have limited the more pronounced inflammatory cascades associated with synthetic materials, which is compatible with the lower pulmonary inflammatory scores observed in this group relative to Group 2. More broadly, large-animal work comparing conventional, revascularized, and bioengineered RLN reconstruction techniques has shown that no single approach fully restores native adductor function [3], reinforcing that RLN repair strategies can have complex and not fully predictable downstream consequences.

Several limitations should be considered. First, the sample size calculation was based on vocal fold mobility, the primary outcome of the parent experiment, and not on pulmonary outcomes; the present lung analysis is a secondary analysis of tissue from those animals and was not powered for the endpoints reported here. With n = 9 per group, effect sizes may be imprecise or overestimated, and the absence of a significant difference (for example, between the fibrin matrix and control groups) does not demonstrate equivalence; indeed, the fibrin matrix group showed intermediate values for edema and parenchymal injury. Second, many endpoints were tested and Holm adjustment was applied only to pairwise comparisons within each endpoint, so all P values, particularly borderline ones and those from the correlation analyses, should be regarded as exploratory. Third, the composite injury scores were defined ad hoc for this study and have not been externally validated, and pulmonary histopathology was graded semi-quantitatively at a single terminal time point. Fourth, we did not perform direct functional swallowing or aspiration testing (e.g., videofluoroscopy or laryngeal electromyography) or measure inflammatory mediators, so the relationship between laryngeal dynamics and pulmonary histopathology remains inferential and the proposed mechanisms were not tested. Fifth, the absence of a non-surgical sham or naive group limits our ability to separate surgical and anesthetic effects from RLN injury-specific pulmonary effects, and no baseline lung histology is available for reference. Sixth, only female rats from a single colony at a single center were studied, which limits generalizability. Seventh, the fibrin matrix was donor-derived from a single separate donor rat and was not quantitatively characterized, so the findings cannot be extrapolated to autologous preparations and donor-to-donor variability could not be assessed. Finally, although histopathological evaluation was performed by a pathologist blinded to group allocation using coded specimens, scoring by a single observer precluded any assessment of

inter-observer reliability, and the operating surgical team could not be blinded given the nature of the interventions.

Despite these limitations, our findings provide preliminary experimental evidence that the strategy chosen for RLN repair may extend beyond local nerve and laryngeal outcomes to influence distant-organ (pulmonary) histopathology. Following experimental RLN transection in rats, isolated primary end-to-end neurorrhaphy was associated with a significantly higher total lung injury score than either unrepaired denervation or repair augmented with donor-derived fibrin matrix; parenchymal and inflammatory scores differed significantly only in some pairwise comparisons, and bronchial luminal diameter did not differ between groups. These findings are exploratory and hypothesis-generating, because the study was not powered for pulmonary outcomes; they suggest that neuroregenerative adjuvants such as fibrin matrix warrant further study as a potential means of limiting pulmonary sequelae along the laryngo-pulmonary axis. Future studies incorporating real-time functional swallowing and respiratory assessment, longer follow-up, larger cohorts, and molecular inflammatory profiling will be needed to confirm these observations, clarify the underlying mechanisms, and help optimize nerve repair strategy in clinical practice.

Methods

Ethical Approval

and Animal Care

The experimental protocol was reviewed and approved by the Local Ethics Committee for Animal Experiments at Necmettin Erbakan University KONÜDAM Experimental Medicine Application and Research Center (Decision No: 2025-032; Date: March 20, 2025). This protocol permitted the procurement of additional target tissues (lungs) from animals utilized in an antecedent project approved by the same ethics committee (“Comparison of Fibrin Matrix and Primary Repair in Recurrent Laryngeal Nerve Reconstruction,” Decision No: 2024 – 113; Date: November 28, 2024), fully adhering to the 3Rs principles (Replacement, Reduction, Refinement). All procedures adhered strictly to the ARRIVE guidelines and the National Institutes of Health Guide for the Care and Use of Laboratory Animals.

Animals and Experimental Grouping

Twenty-seven healthy female Wistar albino rats (aged approximately 3 months at the time of surgery) were used as the experimental animals. One additional donor rat, selected at random before group allocation, was used only to prepare the fibrin matrix (28 animals in total); the donor was not included in any group or analysis. All animals were bred in-house at KONÜDAM (not procured from an external supplier) and were housed three per cage in conventional polycarbonate cages with sawdust bedding, cleaned weekly, under controlled environmental conditions (22 ± 2°C, 50–60% relative humidity, 12-hour light/12-hour dark cycle) with ad libitum access to standard pelleted chow and water. Rats were

randomly allocated into three equal groups (n = 9 per group) using a computer-generated randomization sequence:

- • Group 1 (Control, n = 9): The left RLN was exposed and sharply transected; the surgical bed was closed without neural repair.
- • Group 2 (Primary Repair, n = 9): Following complete left RLN transection, direct end-to-end epineurial neurorrhaphy was performed microsurgically using interrupted 8 – 0 polypropylene (Prolene) sutures under 10× microscopic magnification.
- • Group 3 (Fibrin Matrix, n = 9): Following identical primary neurorrhaphy, a donor-derived fibrin matrix was applied directly over and around the completed anastomosis. The matrix was prepared from approximately 5 mL of fresh whole blood obtained by intracardiac sampling from a single separate donor rat under general anesthesia (intraperitoneal ketamine 80 mg/kg and xylazine 10 mg/kg). The blood was collected without anticoagulant and immediately centrifuged at 400 × g for 10 min using a platelet-rich fibrin (PRF)-based protocol; the fibrin-rich clot formed between the erythrocyte and plasma fractions was separated under sterile conditions and used immediately. For each animal, a visually comparable portion sufficient to cover the repair site without compressing the nerve was applied; its exact weight and dimensions were not measured. The donor rat was not part of the experimental groups or of the present analyses.

Surgical Technique and Endoscopic Evaluation

All microvascular and microsurgical procedures were carried out under an operating microscope by a general surgeon certified in laboratory animal microsurgery. General anesthesia was achieved via intraperitoneal administration of ketamine hydrochloride (80 mg/kg) and xylazine hydrochloride (10 mg/kg). Preoperatively, under the same intraperitoneal ketamine (80 mg/kg) and xylazine (10 mg/kg) anesthesia, baseline bilateral vocal fold mobility was verified transorally using a flexible mini-USB endoscope.

Following skin antisepsis with povidone-iodine in the supine position, a vertical midline cervical incision was performed. Through blunt and sharp dissection in the paratracheal groove, the left RLN was identified, skeletonized, and sharply transected. After executing the group-specific intervention, muscular and subcuticular layers were closed with 4 – 0 polyglactin 910 sutures. Immediate left vocal fold immobility was confirmed endoscopically in all animals before recovery from anesthesia. Postoperative analgesia was maintained with subcutaneous meloxicam (1–2 mg/kg) daily for 5 consecutive days.

Tissue Harvesting and Euthanasia

Surgeries began in January 2025. The postoperative follow-up lasted approximately 3 months, and tissue harvesting was completed toward the end of April 2025. At the end of follow-up, animals were re-anesthetized with intraperitoneal ketamine hydrochloride (80 mg/kg) and xylazine hydrochloride (10

mg/kg), and laryngeal endoscopy was repeated. Via a repeat cervicothoracic approach, the reconstructed nerve segment (with at least 2 mm of healthy margins bilaterally), the intact larynx with bilateral vocal folds, and intact bilateral lung tissue blocks were harvested. Animals were subsequently humanely euthanized by cervical dislocation while still under deep surgical anesthesia (intraperitoneal ketamine 80 mg/kg and xylazine 10 mg/kg).

Histopathological Assessment

Harvested specimens were fixed in 10% neutral buffered formalin for 12–24 hours, routinely dehydrated through graded alcohol series, cleared in xylene, and embedded in paraffin blocks. Consecutive 4-µm-thick sections were cut and stained with hematoxylin and eosin (H&E). All slides were evaluated under light microscopy by a pathologist (N.K.) blinded to group allocation; specimens were presented using coded group numbers only, and the pathologist was not informed which code corresponded to the control, primary repair, or fibrin matrix group. Owing to the nature of the surgical procedures, the operating team could not be blinded to group assignment during the intervention itself.

Pulmonary histopathology was semi-quantitatively assessed across nine parameters: emphysematous changes, atelectasis, peribronchial inflammation, airway obstruction, muscular hypertrophy, alveolar/interstitial edema, parenchymal inflammation, eosinophil infiltration, and vascular congestion. Each parameter was graded as 0 (absent), 1 (mild), or 2 (marked). Bronchial luminal internal diameter was measured quantitatively in millimeters using an ocular micrometer. In nerve sections, axonal density (axons/mm²), inflammatory infiltration, fascicular architecture distortion, vascular proliferation, edema, congestion, and foreign body reaction were documented. In laryngeal sections, intrinsic vocal fold muscle atrophy was evaluated.

Statistical Analysis

An a priori sample-size calculation was based on the primary outcome of vocal fold mobility at 3 months. Assuming expected mobility rates of 0%, 30%, and 70% across the three groups (Cohen's w = 0.61), 27 animals (9 per group) were required to achieve 80% power at a two-sided α of 0.05. The pulmonary analyses reported here are a secondary analysis of tissue obtained from the animals of the parent experiment and were not covered by this calculation. Because multiple pulmonary endpoints were examined and Holm adjustment was applied only to pairwise comparisons within each endpoint, P values for the pulmonary outcomes should be interpreted as exploratory.

To avoid unit-of-analysis bias arising from evaluating bilateral lungs of the same animal as independent observations, the individual animal was designated as the statistical unit. For ordinal pulmonary parameters, the worst-affected side (maximum score between the right and left lungs) was used; for bronchial luminal diameter, the bilateral mean was computed.

Combining several semi-quantitative histopathological parameters into a composite index is an established approach in experimental lung injury research, exemplified by the Ashcroft numerical scale

for pulmonary fibrosis and by the American Thoracic Society workshop report on features and measurements of experimental acute lung injury, both of which aggregate multiple histological features into composite scores [14,15]. Following this general principle, three composite indices were defined for this dataset: a total lung injury score (sum of all nine parameters; range 0–18), a parenchymal injury score (emphysematous changes, atelectasis, edema, and congestion; range 0–8), and an inflammatory injury score (peribronchial inflammation, parenchymal inflammation, and eosinophil infiltration; range 0–6). These composite scores were defined ad hoc for this study and do not correspond to a previously named or externally validated RLN/pulmonary injury scoring system.

Data normality was tested using the Shapiro-Wilk test. Non-parametric continuous and ordinal variables are presented as median [interquartile range, IQR] and mean ± standard deviation (SD). Differences among the three groups were tested using the Kruskal-Wallis test (H). For variables reaching significance ($P < .05$), post-hoc pairwise comparisons were conducted using Dunn's test with Holm-Bonferroni adjustment. Effect sizes were calculated as epsilon-squared (ε^2).

Sensitivity analyses were executed across bilateral mean scores, left-lung scores, and right-lung scores. Bilateral lung symmetry was tested with the Wilcoxon signed-rank test. Exploratory bivariate correlations between pulmonary scores and neuro-laryngeal parameters were assessed using Spearman rank correlation (rho). Airway obstruction showed zero variance (absent in all rats) and was excluded from comparative models. Statistical significance was set at a two-tailed $\alpha = 0.05$. Analyses were performed using SPSS version 26.0 (IBM Corp., Armonk, NY, USA).

Declarations

Acknowledgements

None. During the preparation of this work the author(s) used Claude (Anthropic) in order to assist with literature-search support, language editing, formatting, and manuscript preparation. After using this tool, the author(s) reviewed and edited the content as needed and take(s) full responsibility for the content of the published article.

Authors: please review and adjust the generative AI statement above to accurately reflect your actual use of AI tools before submission.

Author contributions

N.K.: Conceptualization, Methodology, Histopathological evaluation and scoring, Writing – original draft, Writing – review and editing, Project administration, Supervision. A.V.: Conceptualization, Methodology, Surgical interventions and experimental procedures, Formal statistical analysis, Writing – original draft, Writing – review and editing. Ö.K.: Investigation, Data curation, Writing – review and editing. Z.Ç.: Investigation, Data curation, Writing – review and editing. All authors reviewed the manuscript.

Competing interests

The authors declare no competing interests.

Funding

The animal experiments from which the lung tissue was obtained were supported by the Necmettin Erbakan University Scientific Research Projects Coordination Unit (NEU-BAP; grant number 25GAP18002). No additional funding was received for the pulmonary histopathological analysis reported here.

Data availability

The datasets generated and analyzed during the current study are available from the corresponding author upon reasonable request.

References

1. Culp, J. M. & Patel, G. Recurrent Laryngeal Nerve Injury. In StatPearls [Internet] (StatPearls Publishing, (2023).
2. Nekay, E. et al. Anatomical variations of the recurrent laryngeal nerve. in Abstr. 7th Natl. *Endocr. Surg. Congr* 100 (2015).
3. Sand, J. P. et al. Comparison of conventional, revascularized, and bioengineered methods of recurrent laryngeal nerve reconstruction. *JAMA Otolaryngol. Head Neck Surg.* **142**, 526–532 (2016).
4. Paniello, R. C., Rich, J. T. & Debnath, N. L. Laryngeal adductor function in experimental models of recurrent laryngeal nerve injury. *Laryngoscope* **125**, E67–E72 (2015).
5. Choi, J. S. et al. Functional regeneration of recurrent laryngeal nerve injury during thyroid surgery using an asymmetrically porous nerve guide conduit in an animal model. *Thyroid* **24**, 52–59 (2014).
6. Kashiwa, K., Kobayashi, S., Nasu, W., Kuroda, T. & Higuchi, H. Facial nerve reconstruction using a vascularized lateral femoral cutaneous nerve graft based on the superficial circumflex iliac artery system: an application of the inferolateral extension of the groin flap. *J. Reconstr. Microsurg*. **26**, 577–582 (2010).
7. Şentürk, M. et al. Comparison of primary repair and repair with polyglycolic acid coated tube in recurrent laryngeal nerve cuts (an experimental study). *Am. J. Surg.* **219**, 632–636 (2020).
8. Bozkurt, M., Kapı, E. & Külahçı, Y. Conduit applications in peripheral nerve repair, basic and current approaches: a review of the literature. *Turk. J. Plast. Surg.* **17**, 74–83 (2009).
9. Taşkaldıran, A., Koçyiğit, İ. D., Tüz, H., Tekin, U. & Atıl, F. Application of the platelet rich plasma and platelet rich fibrin in oral and maxillofacial surgery. *J. Clin. Sci.* **5**, 947–957 (2011).
10. Erdal, A. İ. The use of erythropoietin and fibrin glue combination in peripheral nerve repair. Medical Specialty Thesis, Gazi University (2019).

11. Senturk, A. et al. Evaluation of the effect of platelet-rich plasma injection after recurrent nerve injury in rats. *Laryngoscope Investig Otolaryngol.* **10**, e70087 (2025).
12. Tsai, M. S. et al. Unilateral vocal fold paralysis and risk of pneumonia: a nationwide population-based cohort study. *Otolaryngol. Head Neck Surg.* **158**, 896–903 (2018).
13. Marik, P. E. Aspiration pneumonitis and aspiration pneumonia. *N Engl. J. Med.* **344**, 665–671 (2001).
14. Ashcroft, T., Simpson, J. M. & Timbrell, V. Simple method of estimating severity of pulmonary fibrosis on a numerical scale. *J. Clin. Pathol.* **41**, 467–470 (1988).
15. Matute-Bello, G. et al. An official American Thoracic Society workshop report: features and measurements of experimental acute lung injury in animals. *Am. J. Respir Cell. Mol. Biol.* **44**, 725–738 (2011).

Figures

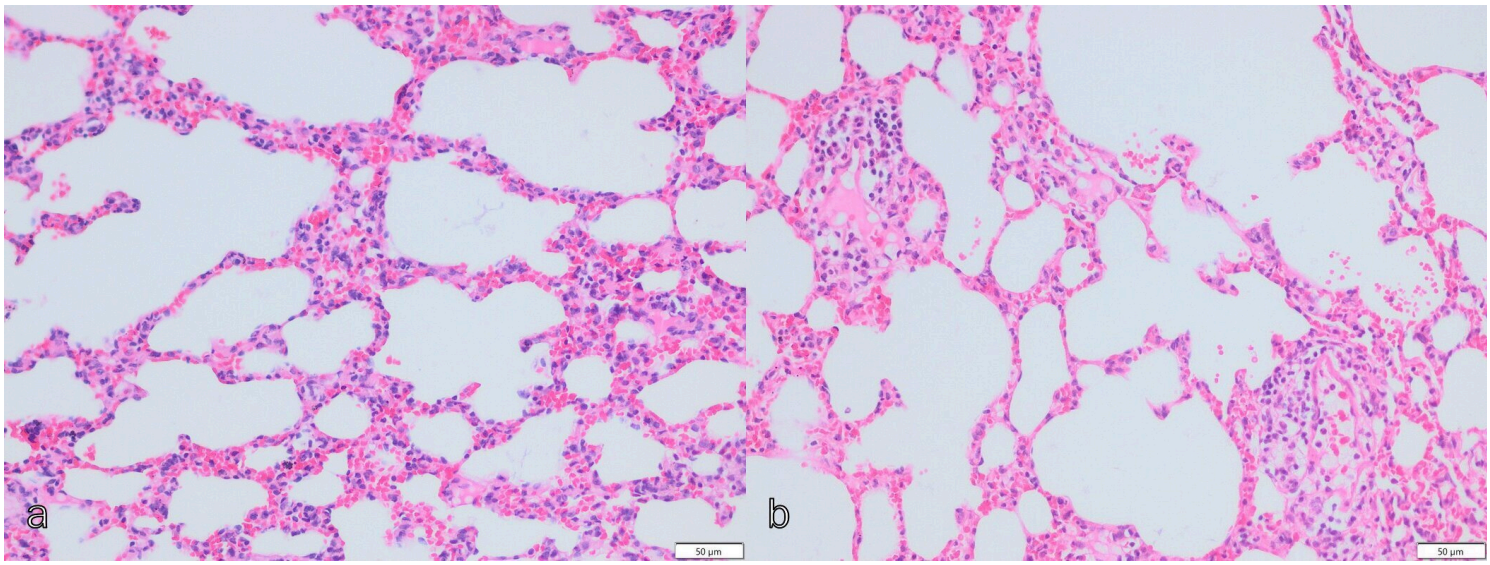


Figure 1

Group 1, unrepaired control. Representative fields illustrating pulmonary edema (a) and parenchymal inflammation (b). (a) Preserved alveolar spaces with mildly thickened, congested interalveolar septa and no intra-alveolar edema fluid. (b) Preserved alveolar architecture with focal small aggregates of mononuclear inflammatory cells (mild parenchymal inflammation) and otherwise thin septa. H&E stain; original magnification ×200; scale bar = 50 µm.

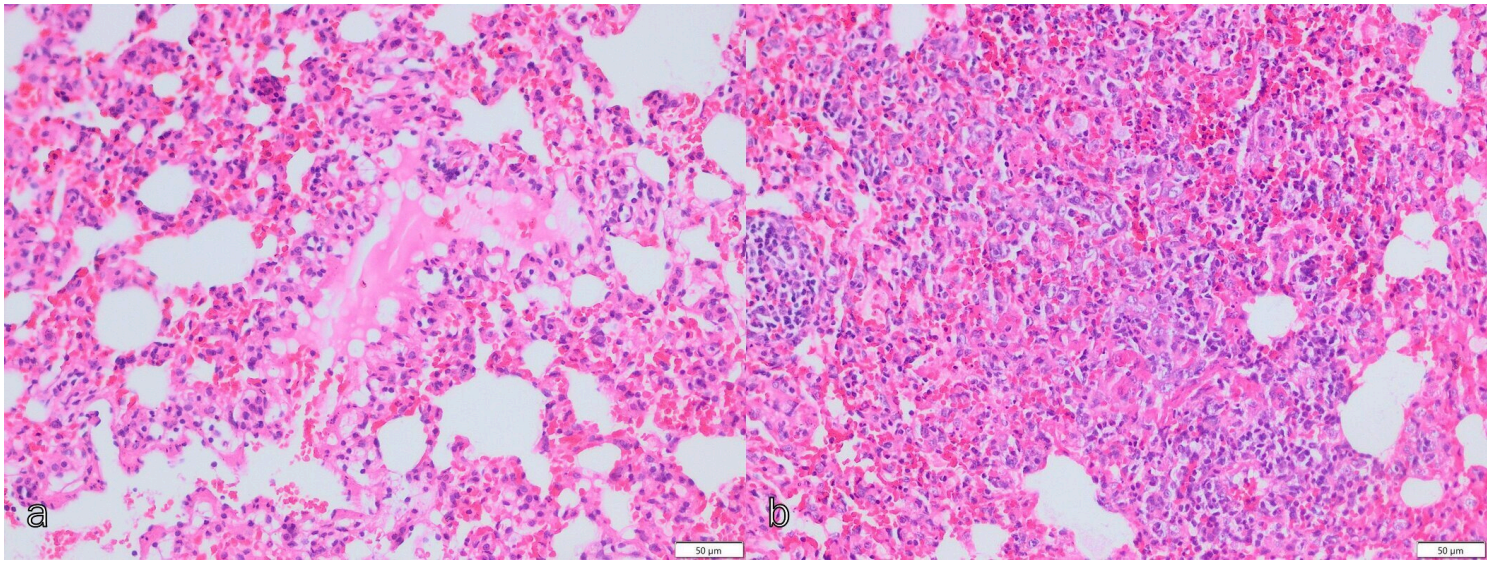


Figure 2

Group 2, primary end-to-end neurorrhaphy. Representative fields illustrating pulmonary edema (a) and parenchymal inflammation (b). (a) Markedly widened, congested interalveolar septa with abundant eosinophilic proteinaceous edema fluid filling the alveolar spaces, consistent with marked alveolar/interstitial edema. (b) Dense, diffuse inflammatory cell infiltration largely obliterates the alveolar spaces, producing marked parenchymal consolidation with associated focal hemorrhage. H&E stain; original magnification ×200; scale bar = 50 µm.

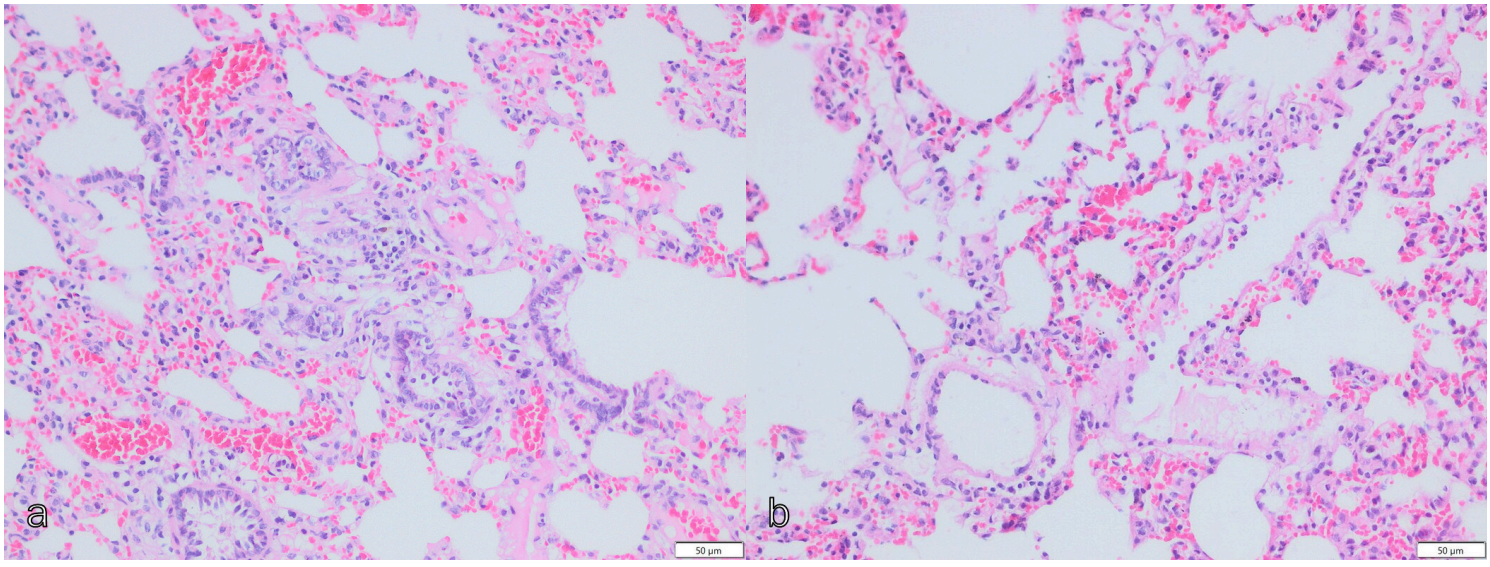


Figure 3

Group 3, neurorrhaphy augmented with donor-derived fibrin matrix. Representative fields illustrating pulmonary edema (a) and parenchymal inflammation (b). (a) Mild-to-moderate interstitial edema with focal septal thickening and vascular congestion, appreciably less extensive than in Group 2. (b) Largely

preserved parenchyma with only sparse interstitial cellularity and no substantial inflammatory infiltrate, in contrast to Fig. 2b. H&E stain; original magnification ×200; scale bar = 50 μm.